SUPPLEMENTAL MATERIAL: On the role played by electrons in the stress-strain curves of ideal crystalline solids

I. ADDITIONAL STRAIN CALCULATION ON AL

Additional strain calculations from 0–1% in 0.1% steps for Al are performed and the corresponding stress-strain curve is shown in Fig.1. They show a linear elastic response with no discernible early non-linearity, even though some experimental works (see ref. 21) report a non-linear stress–strain behavior. This is likely due to the idealized, defect-free model.

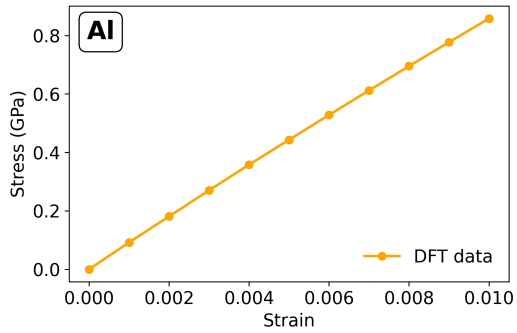

FIG. 1. Stress–strain response obtained from additional tensile strain calculations between 0 and 1% for Al.

II. STRUCTURAL MODIFICATIONS UPON COMPRESSION

As shown in Fig. 2, in all the investigated systems, when the strain $|\epsilon_z|$ is increased, the basis area increases while the cell volumes decreases, consistently with positive isothermal compressibilities and in agreement with what has been found for other materials [1, 2].

As shown in the right panel of Fig. 2, the change in cell volume is strongly influenced by the material under consideration. In fact, the maximum applied strain $\epsilon_z = 0.09$ relates to a small volume reduction for aluminum and copper (1.7%-0.9%), whereas a larger reduction of 6.3% is observed for diamond, exhibiting an almost perfectly linear decrease. This can be linked to the stiffness of the diamond lattice which is not able to accomodate strain by deforming and expanding its basis cell area as much as Al and Cu do. As will be shown in the next section, the higher $|\Delta V/V_0|$ of diamond are associated to much larger stress $|\sigma_{zz}|$ by which this material opposes the given target strains. Importantly, despite the fact that full relaxation is allowed concerning the atomic positions, no significant displacement is found at any strain even for the metals that display the elastic-plastic transition: Cu atoms deviate at most of 0.34% with respect

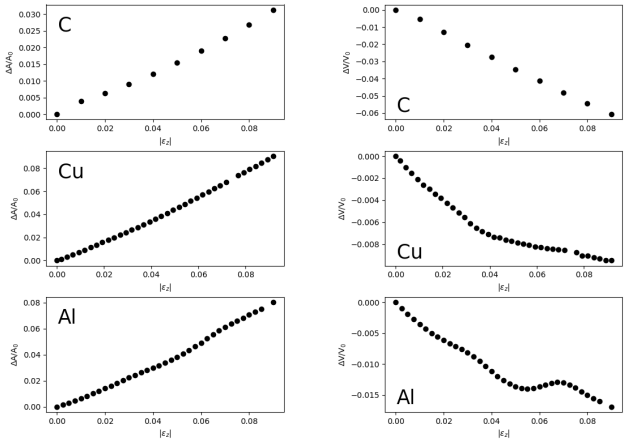

FIG. 2. Left: variations of the basis cell area $\Delta A/A_0$ with respect to the vertical strain $|\epsilon_z|$. Right: variations of the cell volume $\Delta V/V_0$ with respect to vertical strain $|\epsilon_z|$. A_0 and V_0 denote the equilibrium area and volume.

to their ideal position in the x and y directions and 0.1% in the z direction; Al atoms maximum relative displacements are 0.16% in the x and y directions and 0.28% along z; whereas the maximum relative displacement of C atoms are of the order of 10^{-5} and 10^{-3} in the x and y, and z direction respectively.

III. ELASTIC PROPERTIES

The Young's modulus E has been calculated by fitting the linear region close to the origin of the stress strain curves where the materials obey Hooke's law $\sigma = E \cdot \epsilon$. The results are reported in Tab.I and agree with experimental observations.

Poisson's ratio ν, the ratio between transverse and longitudinal (with respect to the load direction) strain, in our case $\nu = -\epsilon_x/\epsilon_z$, is a measure of how much a material resists in deforming upon uniaxial stress: the higher ν, the higher the material resistance to changes in volume. For a perfectly incompressible, isotropic material the Poisson ratio should reach the ideal value of 0.5. ν provides insights into the nature of atomic bonding and chemical properties of a solid: Poisson's ratio values for covalent materials are typically around $\sim$0.1, $\sim$0.25 for ionic materials, and vary between 0.28 and 0.42 for metals [3]. Consistently, the calculated Poisson's ratio for diamond, in the limit of 0 strain is $\sim$0.1, reflecting its covalent bonding nature, in agreement with experiments [3], and Poisson's ratios of aluminum and copper are $\sim$0.32 and $\sim$0.34. The computed values are in excellent agreement with experiments as shown in Tab.I. As

shown in Fig.3, Poisson's ratio increases with pressure for all materials under investigation. Similar trends have been found employing classical force fields for wurtzite aluminum nitrate and diamond [4, 5], and using DFT for Ni_3X compounds [1] under load.

Material	E (GPa)	E_{exp} (GPa)	ν	ν_{exp}
C	1068	700-1200	0.107	0.10-0.30
Cu	97	110	0.341	0.34
Al	82	69	0.326	0.33

TABLE I. Comparison between calculated and experimental values of Young's modulus E and Poisson's ratio ν for Al, Cu, C. Experimental values are obtained from Ref.[6].

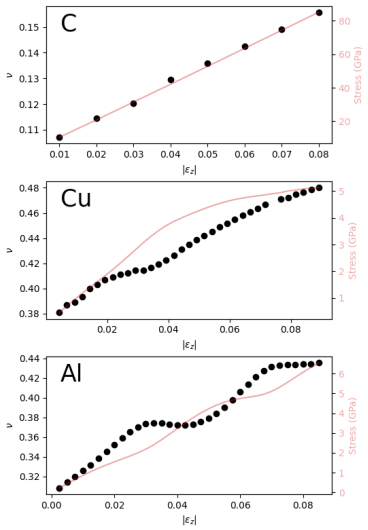

FIG. 3. Poisson's ratio ν against vertical strain $|\epsilon_z|$ for C (top), Cu (center) and Al(bottom). In red, as a guide to the eye, also the stress values are reported.

IV. SYMMETRY ANALYSIS UNDER UNIAXIAL LOAD

Structural distortions and symmetry breaking were assessed using ASE [7] and spglib [8], two Python libraries for atomistic modeling and crystallographic symmetry analysis. For each load, the space group of the relaxed bulk cell was determined and the set of equivalent atoms identified. As expected under uniaxial loading, the lattice exhibits a uniform tetragonal metric distortion (change in c/a) relative to the unstrained Fm-3m reference. Moreover, within that tetragonal phase, all atoms remain on a single crystallographic site (one equivalence class). This result is robust with respect to symmetry tolerances over physically meaningful ranges (distance tolerance $10^{-3} - 10^{-2}$ Å and angle tolerance of 0.5°). Only when the distance threshold is forced down to 10^{-7} Å atomic sites become "inequivalent", which reflects numerical noise rather than a real symmetry change. Thus, no load-induced breaking of atomic equivalence is observed and the changes are attributed to the electronic system rather than to a hidden structural symmetry lowering.

V. IDENTIFICATION OF AL CRITICAL POINTS

To identify the critical point associated to the second order phase transition of Al, the first and second order derivatives of the thermodynamic potential F are analyzed. From the first derivative of F (Fig.4(a)), linear regressions are performed over two distinct strain intervals, $0.015 \leq \epsilon \leq 0.0225$ and $0.035 \leq \epsilon \leq 0.045$. The critical point is defined as the intersection between the two resulting lines, yielding a value of ϵ=0.03. By fitting the second derivative of F (Fig.4(b)) with a 11th-degree polynomial in the range $0.0015 \leq \epsilon \leq 0.05$, the local minimum and maximum of the interpolated curve, occurring at $\epsilon_{min} = 0.022$ and $\epsilon_{max} = 0.0389$ respectively, are identified. The average of these two values, ϵ=0.03, provides an alternative estimate of the critical point. Both approaches converge to a consistent estimate of the critical point at 0.03 strain, marking the second order phase transition.

The critical point associated to the first order phase transition of Al is identified by interpolating the second derivative of F with a 13th-degree polynomial in the range $0.025 \leq \epsilon \leq 0.085$ (Fig.5). The two local maxima at ϵ=0.04 and 0.0775 identify the range of the transition, while the minimum at ϵ=0.0625 represents the critical point.

VI. GIBBS FREE ENERGY ANALYSIS FOR AL

In Fig.6(a) the Gibbs free energy of Al as a function of the natural variable stress×area conjugated to l_z is plotted, whereas its first and second order derivatives are shown in panel (c) and (b), respectively.

VII. AL DOS ANALYSIS

The behaviour of Al density of states calculated for different strains around the critical value of 3%, which marks the second order phase transition, is shown in Fig.7. In this case, there are no Van Hove singularities crossing the Fermi level, suggesting that no Lifshitz transition is occurring.

In Fig.8, the evolutions of the Fermi level (panel(a)) and that of the DOS at the Fermi level (panel (b)) with strain for the case of Al are shown. The black dashed lines delimit the ranges in which the transitions occur, whereas the green lines are the critical points identified by the

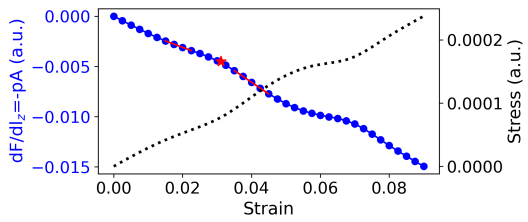

(a)

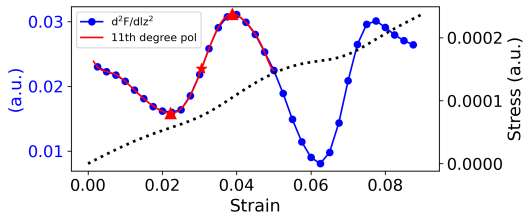

(b)

FIG. 4. (a) First order derivative of Helmholtz free energy F as a function of strain. Linear fits are shown as red lines. (b) Second order derivative of Helmholtz free energy F as a function of strain. The fit performed with a 11th-degree polinomial is shown as a red line and the local minimum and maximum are marked with red triangles. In all panels the critical point is marked with a red star and stress values are reported as a black dotted line referring to the right axis labels.

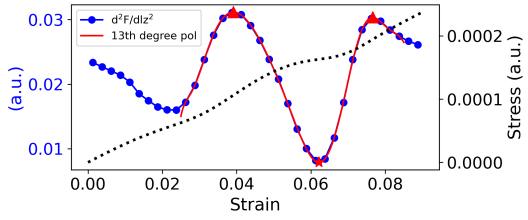

FIG. 5. Second order derivative of Helmholtz free energy F as a function of strain. The fit performed with a 13th-degree polinomial is shown as a red line, the local maxima are marked with red triangles, while the critical point is indicated with a red star. Stress values are reported as a black dotted line referring to the right axis labels.

analysis of the thermodynamic potential as presented in the previous section. At around 3% strain, i.e. at the location of a non analytic point that has been previously identified as reminiscent of a second order phase transition, there is a change in slope in the Fermi level. Whereas $\sim$ 6% strain, where the behavior of the thermodynamic potential suggested a first order phase transition, is between a high/low Fermi level (or a low/high DOS(E_F)) regimes.

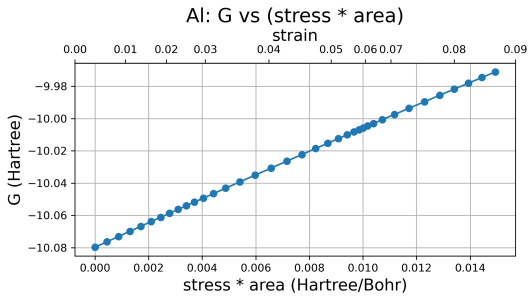

(a)

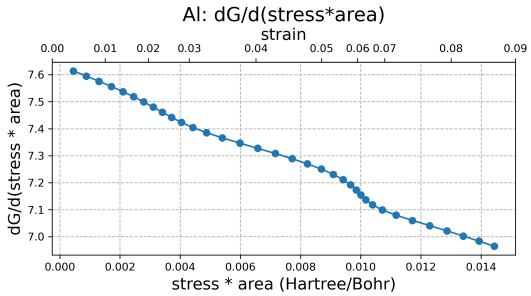

(b)

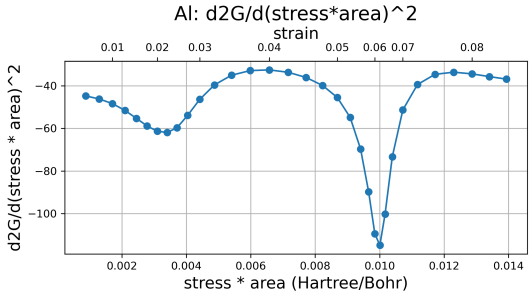

(c)

FIG. 6. Gibbs free energy (a) and its first (b) and second (c) order derivatives as a function of the natural variable stress$\times$area.

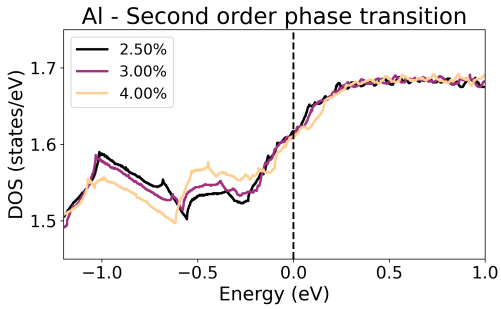

FIG. 7. Al DOS for strain values around the critical $\epsilon_z = 0.03$.

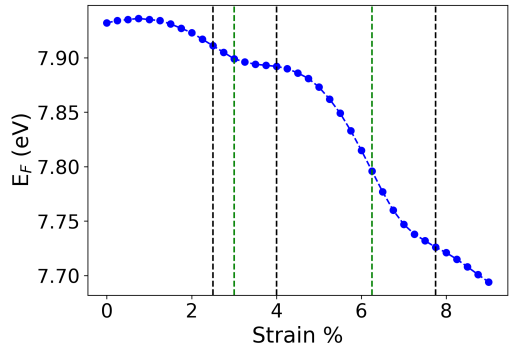

(a)

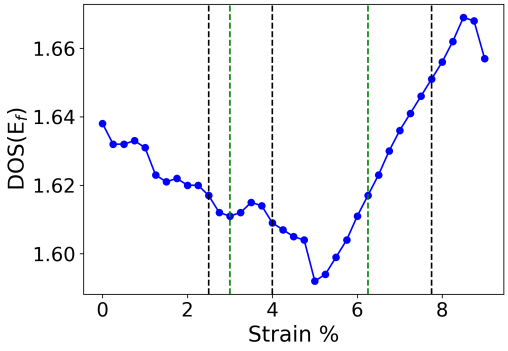

(b)

FIG. 8. (a) Fermi energy and (b) value of the density of states at the Fermi level of Al as a function of strain. The black dashed lines delimit the ranges in which the transitions occur, whereas the green lines are the critical points identified by the analysis of the thermodynamic potential.

VIII. AL BAND STRUCTURE

The complete Al band structure computed at different strains is shown in Fig. 9. The colored bands are those discussed in the main text, as they cross the Fermi level upon increasing strain. An additional crossing occurs at the X_1 point, where the minimum of two degenerate bands (blue and orange) shifts from above to below E_F, i.e., from unoccupied to occupied, at $\epsilon_z \sim 5\%$. This further contributes to the electronic rearrangement taking place at X in the same strain range.

IX. REAL-SPACE CHARACTER OF THE STATES CROSSING E_F

Here we report the planar-averaged charge density along the z direction of those Kohn-Sham (KS) states representing the band extrema crossing E_F. By $n = 6, 7, 8$, we refer to the green, blue and orange bands of Fig.9. In Fig.10, charge profiles of the KS states crossing the Fermi level at $\epsilon_z \sim 5\%$ are plotted. As mentioned in the main text, it is interesting to point out that the KS states belonging to band 7 (blue) and 8 (orange) crossing E_F at the X point change their character. Indeed, they switch from being predominantly localized on the atomic planes to a more interlayer-localized distribution. In contrast, the state corresponding to the minimum of band 7 (blue) at the X-P side keeps accumulating charge between atomic planes. The degenerate states at X_1 that become occupied at $\epsilon_z \sim 5\%$ do not show any change in character. A similar conclusion holds for the states corresponding to the minimum and maximum of band 7 (blue) and 6 (green) at the Γ-X side, that cross E_F at $\epsilon_z \sim 3\%$: they both preserve their localization on atomic planes (see Fig.11).

[1] H. Hou, Z. Wen, Y. Zhao, L. Fu, N. Wang, and P. Han, First-principles investigations on structural, elastic, thermodynamic and electronic properties of Ni_3X (X=Al, Ga and Ge) under pressure, Intermetallics **44**, 110 (2014).

[2] F. Nestola, G. Zaffiro, M. L. Mazzucchelli, P. Nimis, G. B. Andreozzi, B. Periotto, F. Princivalle, D. Lenaz, L. Secco, L. Pasqualetto, A. M. Logvinova, N. V. Sobolev, A. Lorenzetti, and J. W. Harris, Diamond-inclusion system recording old deep lithosphere conditions at Udachnaya (Siberia), Scientific Reports **9**, 12586 (2019).

[3] G. N. Greaves, A. L. Greer, R. S. Lakes, and T. Rouxel, Poisson's ratio and modern materials, Nature Materials **10**, 823 (2011).

[4] E. Güler and M. Güler, High pressure elastic properties of wurtzite aluminum nitrate, Chinese Journal of Physics **52**, 1625 (2014).

[5] E. Güler and M. Gueler, Elastic and mechanical properties of cubic diamond under pressure, Chinese Journal of physics **53**, 195 (2015).

[6] W. Callister Jr. and D. Rethwisch, *Materials Science and Engineering: An Introduction*, 10th ed. (Wiley).

[7] A. Hjorth Larsen, J. Jørgen Mortensen, J. Blomqvist, *et al.*, The atomic simulation environment—a python library for working with atoms, Journal of Physics: Condensed Matter **29**, 273002 (2017).

[8] A. Togo, K. Shinohara, and I. Tanaka, Spglib: a software library for crystal symmetry search, Science and Technology of Advanced Materials: Methods **4**, 2384822 (2024).

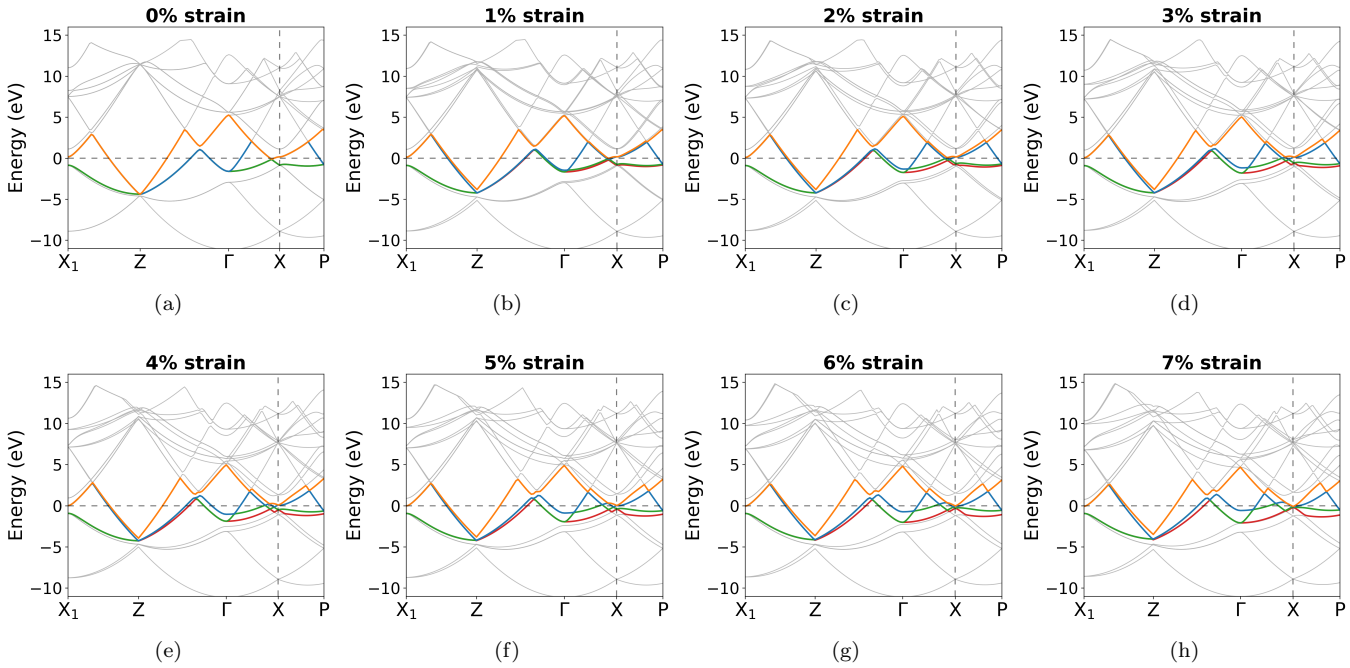

FIG. 9. Evolution of Al band structure upon strain along the X_1-Z-Γ-X-P k-path. The Fermi level is set at 0 and is marked by the horizontal dashed line. The vertical dashed line marks the X point. Coloured bands corresponds to the ones reported in the main text.

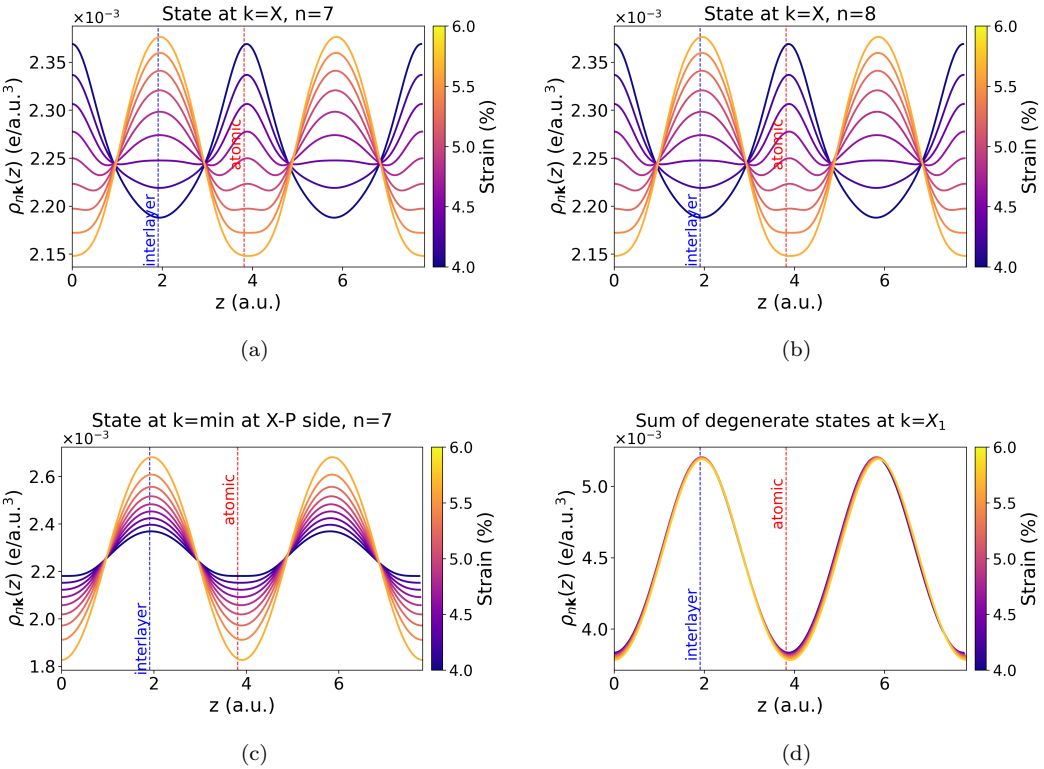

FIG. 10. $\rho(z)$ of the Kohn-Sham states crossing the Fermi level at strain $\sim 5\%$.

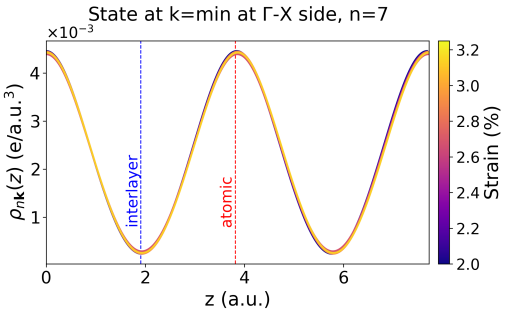

(a)

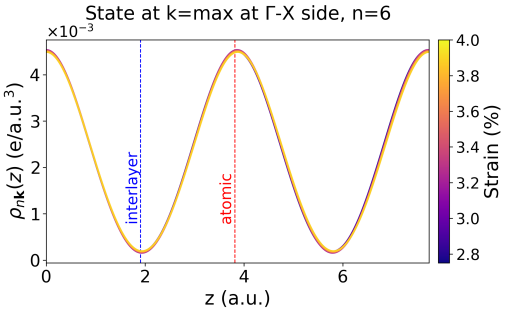

(b)

FIG. 11. $\rho(z)$ of the Kohn-Sham states crossing the Fermi level at strain $\sim 3\%$.